[Scanning Microscopy](https://digitalcommons.usu.edu/microscopy)

Volume 1995
Number 9 *Luminescence*

Article 6

1995

Scanning Tunneling Microscope-Induced Luminescence Spectroscopy on Semiconductor Heterostructures

M. Pfister
Zurich Research Laboratory

M. B. Johnson
Zurich Research Laboratory

U. Marti
Ecole Polytechnique Fédérale

S. F. Alvarado
Zurich Research Laboratory, alv@zurich.ibm.com

H. W. M. Salemink
Zurich Research Laboratory

See next page for additional authors

Follow this and additional works at: https://digitalcommons.usu.edu/microscopy

Part of the Biology Commons

Recommended Citation

Pfister, M.; Johnson, M. B.; Marti, U.; Alvarado, S. F.; Salemink, H. W. M.; Martin, D.; Morier-Genoud, F.; and Reinhart, F. K. (1995) "Scanning Tunneling Microscope-Induced Luminescence Spectroscopy on Semiconductor Heterostructures," *Scanning Microscopy*: Vol. 1995 : No. 9 , Article 6.
Available at: https://digitalcommons.usu.edu/microscopy/vol1995/iss9/6

This Article is brought to you for free and open access by the Western Dairy Center at DigitalCommons@USU. It has been accepted for inclusion in Scanning Microscopy by an authorized administrator of DigitalCommons@USU. For more information, please contact digitalcommons@usu.edu.

UtahStateUniversity
MERRILL-CAZIER LIBRARY

Scanning Tunneling Microscope-Induced Luminescence Spectroscopy on Semiconductor Heterostructures

Authors

M. Pfister, M. B. Johnson, U. Marti, S. F. Alvarado, H. W. M. Salemink, D. Martin, F. Morier-Genoud, and F. K. Reinhart

This article is available in Scanning Microscopy: https://digitalcommons.usu.edu/microscopy/vol1995/iss9/6

Scanning Microscopy Supplement 9, 1995 (Pages 87-92)
Scanning Microscopy International, Chicago (AMF O'Hare), IL 60666 USA

0892-953X/95$5.00+.25

SCANNING TUNNELING MICROSCOPE-INDUCED LUMINESCENCE SPECTROSCOPY ON SEMICONDUCTOR HETEROSTRUCTURES

M. Pfister[1,2], M.B. Johnson[1], U. Marti[2], S.F. Alvarado[1,*],
H.W.M. Salemink[1], D. Martin[2], F. Morier-Genoud[2] and F.K. Reinhart[2]

[1]IBM Research Division, Zurich Research Laboratory, 8803 Rüschlikon, Switzerland
[2]Institut de Micro- et Opto-électronique, Ecole Polytechnique Fédérale, 1015 Lausanne, Switzerland

Abstract

Scanning tunneling microscope (STM)-induced luminescence is explored as a technique for the characterization of semiconductor quantum wells and quantum wire heterostructures. By injecting minority carriers into the cleaved cross section of these structures, luminescence excitation on a nanometer scale is demonstrated. Using spectrally resolved STM-induced luminescence for the tip placed at various positions across the cleaved heterostructure, it is possible to obtain local spectroscopic information on closely spaced quantum structures.

Key Words: Scanning tunneling microscopy, tunneling-induced luminescence, quantum wires.

*Address for correspondence:
S.F. Alvarado
IBM Research Division
Zurich Research Laboratory
CH-8803 Rüschlikon
Switzerland

Telephone number: +41-1-724-8216
FAX number: +41-1-724-0809
E.mail: alv@zurich.ibm.com

Introduction

Scanning tunneling-induced luminescence (STL) [1, 3, 10] is a novel technique that overcomes some limitations of imaging and spectroscopic analysis of conventional cathodoluminescence, for which the resolution is limited by the large thermalization volumes of the high-energy (several keV) electrons [6]. By applying STL to cleaved cross sections of semiconductor heterostructures, nanometer-scale local excitation is possible. The technique is especially useful for the analysis of low-dimensional semiconductor structures such as quantum wells (QW), wires (QWR) and dots. Recently, cross-sectional scanning tunneling microscopy (STM) has been applied to the study of cleaved III-V semiconductor heterostructures [2, 7, 8]. In these studies, structural and electronic properties of heterostructures can be determined on an atomic scale. Combining the induced luminescence with this technique offers the possibility to study the optical properties of heterostructures as well, including single QWR.

In this paper, we show results obtained for cross-sectionally cleaved GaAs QW and QWR heterostructures embedded in $(AlAs)_4(GaAs)_8$ superlattice (SL) barriers. The wavelength-resolved luminescence spectra taken at different positions across the planar SL structure show that it is possible to obtain local spectroscopic information on closely spaced quantum structures.

Experimental

Samples

The two samples discussed in this paper consist of a series of QWR and QW embedded in $(AlAs)_4(GaAs)_8$ SL barriers. The samples are grown by molecular beam epitaxy in the same growth run using a patterned GaAs substrate for the QWR sample and a planar one for the QW sample. Patterning is achieved by holographic lithography and wet-etching to form an array of V-grooves of 190 nm periodicity and side wall facets with orientations close to {111}B planes [9]. Each barrier consists of 5.5 periods of a SL with a total thickness

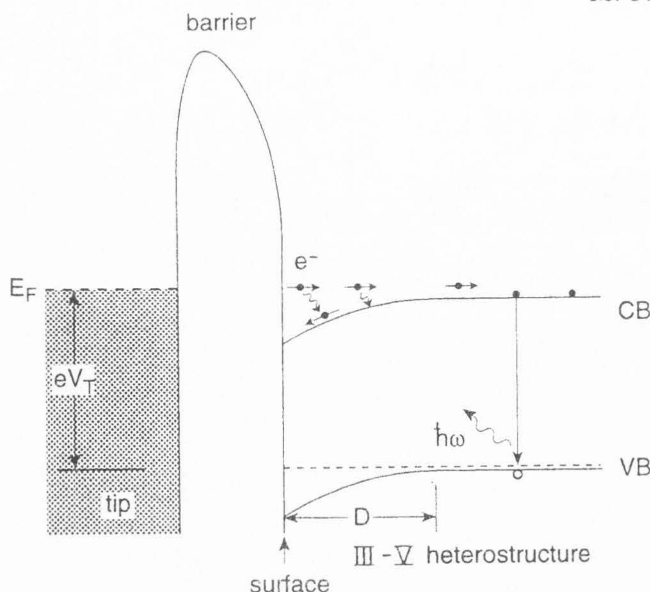

Figure 1. Schematic of the tip/semiconductor junction showing the tunnel injection process for electrons (e^-) into the conduction band (CB) of a *p*-type direct-gap semiconductor. *D* is the width of the surface depletion layer resulting from a partial Fermi level (E_F) pinning at the surface. Photon emission ($\hbar\omega$) originates from the non-depleted subsurface region when an electron recombines radiatively with a hole from the valence band (VB).

of 18 nm. The wells are produced by growing a nominally 5-nm-thick GaAs layer followed by a 120 second growth interruption. This sequence is repeated 11 times with the substrate temperature increasing from 550 to 700°C between QW1 and QW8; for QW9 to QW11, the substrate temperature was 600°C. The substrate is *p*-doped (Zn) at 1 x 10^{18} cm^{-3}, and the epitaxial structure is nominally homogeneously Be-doped at 7 x 10^{18} cm^{-3}, calibrated for a growth temperature of 600°C.

Structural analysis plus dopant profiling are performed with high-resolution STM on an adjacent QWR sample, and have been published elsewhere [11]. The doping concentration in the QWR and QW and in the SL barriers is found to decrease from QW1 to QW8 as the growth temperature is increased to 700°C, whereas the last three QW (QW9 through QW11) grown at 600°C again show higher doping levels. In addition, the QWR and QW thicknesses decrease with increasing temperature owing to strong Ga desorption during the growth interruption at high growth temperatures. For the last three QW grown at 600°C, the nominal thickness of 5 nm was reestablished.

STL-STM system

Samples were cleaved in a ultra high vacuum scanning tunneling microscope (UHV-STM) chamber with a base pressure of 5 x 10^{-10} mbar. This results in an atomically flat (011) surface. Slight oxidation (more on AlGaAs than on GaAs) occurs between cleavage and measurement. This leads to a partial Fermi-level pinning of the (011) surface, which gives rise to a surface depletion layer at the surface of the cleaved sample. STM measurements are performed in constant current mode with various currents up to 1 nA and typical sample voltages of +2.0 V. The tunneling-induced light is collected by a lens with F = 1.12, situated 25 mm from the tip apex, providing a full collection cone of 45°. The optical axis forms an angle of 45° towards the sample surface normal (the UHV chamber used for these measurements is different from that used previously [1], where the angle between the optical axis and the sample normal was about 60°). The collimated light is coupled outside the UHV chamber through a view-port and refocused onto a Si avalanche diode photon counting module. Plotting the integral luminescence intensity as a function of the scanning tip position on the sample produces a photon map of the cross-sectional heterostructure which is measured at the same time as the topography map. For the wavelength-resolved spectra, the light is refocused onto the circular end of a quartz fiber optic bundle, while at the other end, the fibers are in linear arrangement and form the entrance slit to the spectrometer. The spectra are recorded using a liquid nitrogen cooled charged couple device (CCD) camera. The typical acquisition time for recording spectra of the room-temperature luminescence with tunneling currents in the nanoampere range and voltage below the *e-h* pair ionization threshold is about 30 seconds.

Results and Discussion

The processes involved in STL for a *p*-doped semiconductor with Fermi level pinning at the surface are shown in the schematic band diagram of Figure 1. These processes are: electron injection into the bulk-like flat-band region involving tunneling across the vacuum barrier, and then quasiballistic transport across the surface depletion layer (D); thermalization of the hot electrons to the bottom of the conduction band (CB) in the flat-band region; diffusion of the electrons; and finally, radiative recombination of the electron with a hole from the valence band. Generally, the luminescence intensity depends on (1) the efficiency of carrier injection into the flat-band region and (2) the competition between radiative and non-radiative processes in this region below the surface depletion layer. The efficiency of carrier injection in (1) strongly depends on the excess energy above the CB of the injected electron (therefore decreasing strongly when moving at constant injection

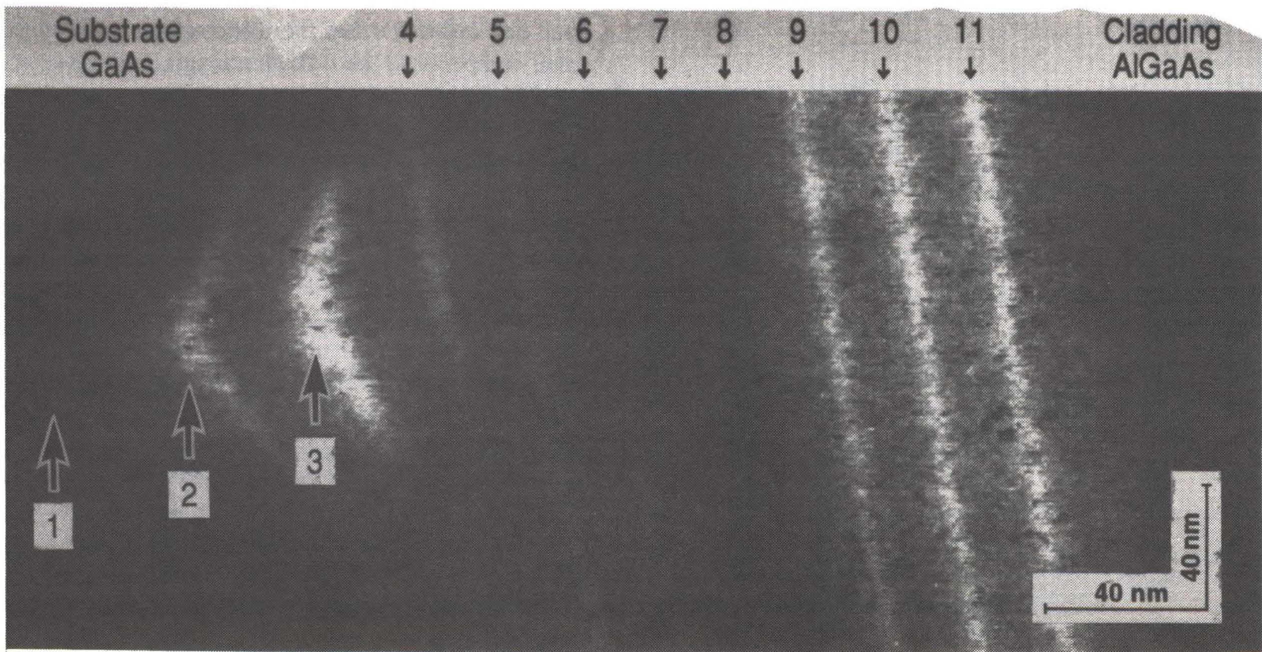

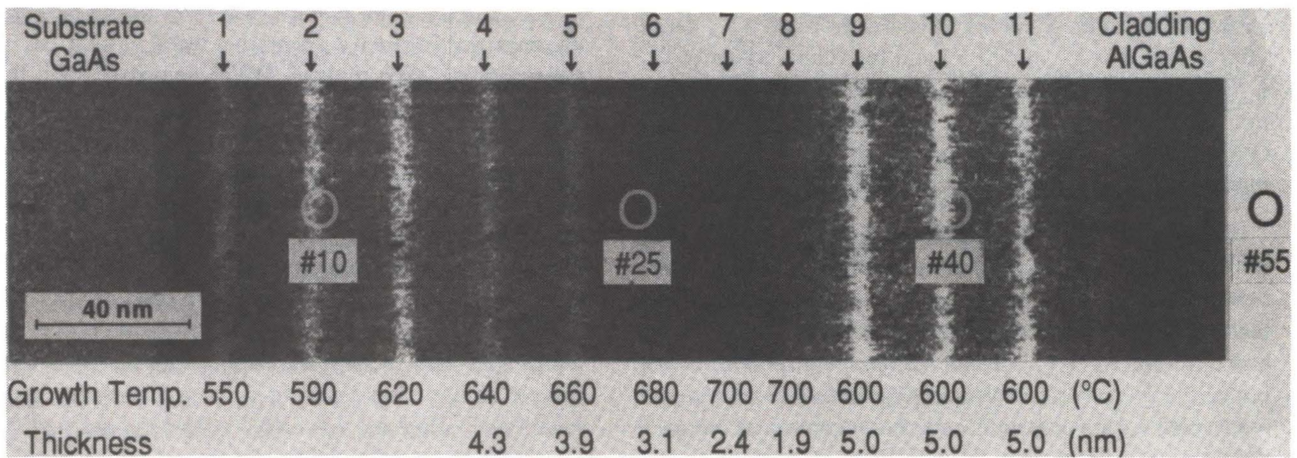

Figure 2 (top). Scanning tunneling-induced luminescence map of a 310 x 180 nm^2 cross section of a quantum wire sample taken at constant bias (V_s = 2.2 V) and tunneling current (I_t = 1.0 nA). The gray scale ranges from 0 (black) to 7500 (white) counts per second. The quantum wires (1-3) are labeled in the figure, and the wells are labeled above. Quantum wire #1, close to the etched interface, has a very low luminescence yield.

Figure 3 (bottom). Scanning tunneling-induced luminescence map of a 300 x 70 nm^2 cross section of the planar quantum well sample taken at constant bias (V_s = 2.2 V) and tunneling current (I_t = 1.0 nA). The gray scale ranges from 0 (black) to 2500 (white) counts per second. The QW are labeled above, and their growth temperatures together with the QW thicknesses measured by cross-sectional STM are shown below the image. The circles mark the positions where the four spectra shown in Figure 4 were recorded.

---

energy from a lower to a higher band gap material) and on the doping of the material. With increasing excess energy, more electrons have sufficient energy to cross the depletion layer. Electrons that have lost too much energy during scattering events will drift in the electric field of the space-charge region back to the surface where they recombine non-radiatively. The width of the depletion layer is proportional to $(1/p)^{-1/2}$ (for a pinned Fermi level and a doping concentration of p = 7 x 10^{18} cm^{-3}, the depletion width is about 12 nm). For lower-doped material, the depletion layer is larger; therefore, fewer carriers can be expected to be transported through

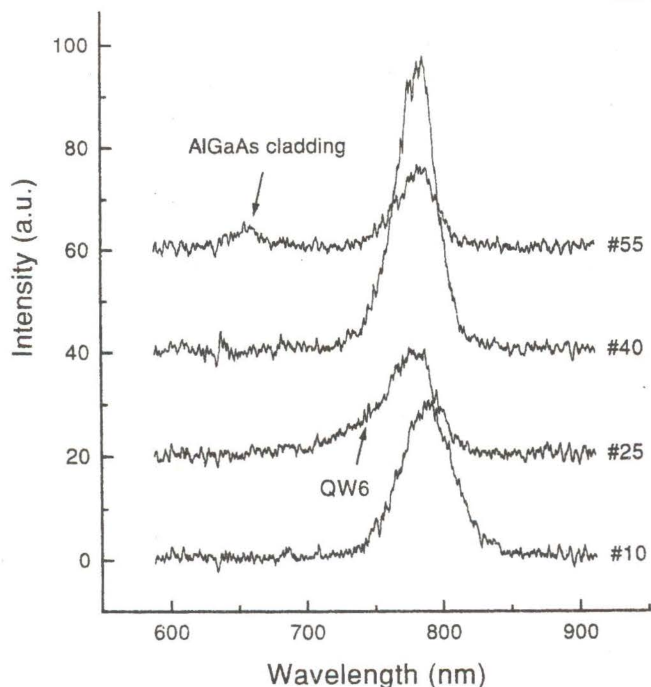

Figure 4. Tunneling-induced luminescence spectra recorded at the four positions indicated in Figure 3. The sample bias was V_s = 3.0 V) and the tunneling current I_t = 1.0 nA. The thermalization volume at 3.0 V injection energy is comparable to the distance between the QW. Therefore, luminescence from QW of different thicknesses can contribute to one spectra, cf. #25.

---

it. This is an important reason for the lower luminescence yield at lower doping concentrations (one effect that might lower the luminescence yield at higher doping concentration is the reduced ballistic transport due to impurity related scattering; compared to other scattering mechanisms, this contribution is not expected to be important). The internal quantum efficiency is determined by the competition between radiative recombination and non-radiative processes, such as recombination at deep levels due to defects in the bulk-like flat band region. The radiative lifetime of minority electrons in *p*-doped GaAs is strongly dependent on the hole concentration. Up to a Be doping level of 10^{19} cm^{-3}, we can expect that the radiative lifetime decreases with increasing doping concentration [5]. Finally, as with cathodoluminescence, the resolution of the technique is largely governed by the thermalization volume and minority carrier diffusion. In STL, where the electron energies are close to the CB, the thermalization volume is about two orders of magnitude smaller than is the case for cathodoluminescence, for which electron energies are typically 0.5 to 20 keV. Minority carrier diffusion in three, two or one dimension may take place, depending on the heterostructure configuration. Radiative recombination will preferentially occur in the lowest band gap material when the thickness of the barriers is small compared to the diffusion length in the barrier.

Figures 2 and 3 show luminescence maps of 310-nm-wide areas of the cleaved cross section of the QWR and the QW samples, respectively. Both images were taken at constant sample bias (V_s = 2.2 V) and tunneling current (I_t = 1.0 nA). The integrated luminescence intensity is given by a gray scale; for the range, see figure captions. The bright regions are associated with QW and QWR, as labeled. The nominal growth temperatures and QW thicknesses measured on the planarized part of a QWR sample by cross-sectional STM are indicated in Figure 3. The contrast between the GaAs well wires and SL barriers is mostly due to the large difference of the injection efficiency between these regions as a result of the difference in their band gaps. Thus, the shape of the bright regions in the QWR sample indicates the V-shaped cross section of the GaAs wires. These shapes are in agreement with the atomically resolved cross-sectional STM results [11]. Two striking features are associated with the relative brightness of the QW and QWR. The first is the reduced luminescence intensity from the wells grown at high temperature (QW5 through QW8) compared with those grown at lower temperatures above and below. As discussed above, these wells are thinner and less doped due to the high growth temperature. Both of these properties lead to reduced luminescence: For thinner QW, the increase in the confinement energy leads to a decrease in the excess injection energy above the lowest quantum level, resulting in a reduction in carrier injection. Lower doping results in a thicker depletion region, which therefore reduces the carrier injection efficiency. Lower doping also leads to a longer minority carrier radiative lifetime, which allows non-radiative recombination paths to dominate. Furthermore, the increased importance of interface defects in very thin QW may contribute to the low luminescence yield. The second feature is the lower intensity of QW1 compared with QW2 and QW3 (Fig. 3) or, even more dramatic, the larger differences in intensities between QWR1, QWR2 and QWR3 (Fig. 2). These results are attributed to a shortened non-radiative lifetime due to an increased concentration of non-radiative recombination centers such as crystallographic defects or deep impurities. These centers occur because no buffer layer was grown on the substrate, and thus the QWR and QW closest to the substrate interface would be expected to have a higher concentration of such defects.

Across the planar heterostructure shown in Figure 3, a series of 60 wavelength-resolved spectra are taken by moving the tip in steps of 5 nm between every acquisition. The tunneling conditions were V_s = 3.0 V with

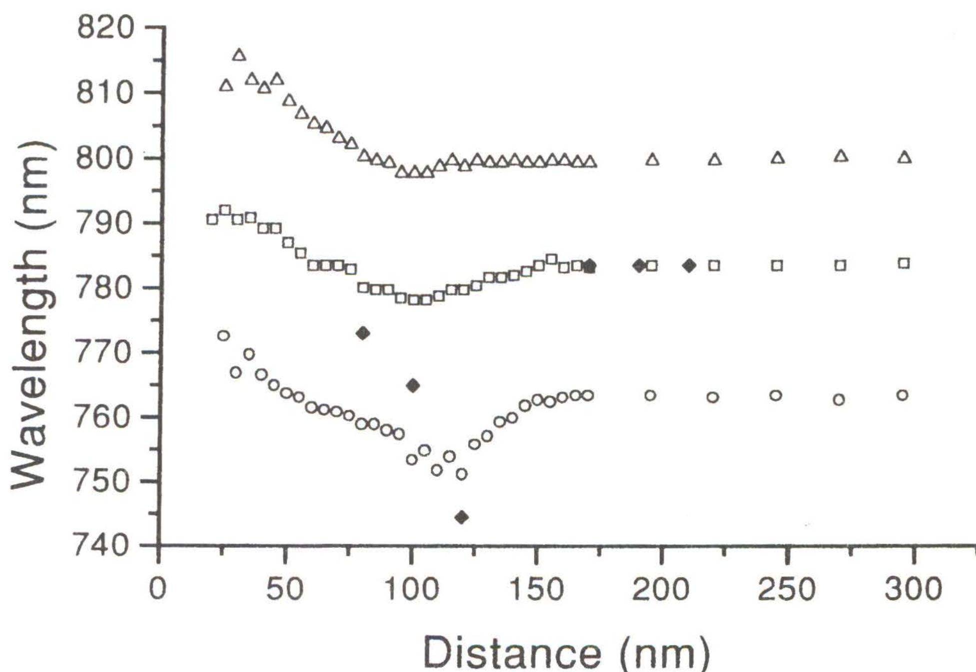

Figure 5. Observed peak wavelength (squares) of the tunneling-induced luminescence as a function of the tip position over the cross section of the heterostructure. Triangles and circles show the wavelength at half maximum on the low and high-energy side of the peak, respectively. The distance between consecutive spectra is 5 nm (only every fifth measurement is shown from spectrum #35 on). The diamonds indicate the expected peak wavelengths for QW #4 to #6 and #9 to #11 of Figure 3.

a tunneling current of I_t = 2 nA. In the present investigation, a higher sample voltage was used than shown in Figure 3. Although this gives rise to lower luminescence contrast due to larger thermalization volumes, a larger luminescence signal is generated. With these injection parameters, an acquisition time of 30 seconds was required for each spectrum. By comparing the peak heights of the recorded spectra to the luminescence map in Figure 3, the position that each spectrum was taken can be determined within 5 nm. Figure 4 shows four different spectra selected from the set of 60 spectra, taken at positions indicated in Figure 3. Spectrum #10 is taken close to the second QW (QW2, 590°C); it shows the characteristic shape for room-temperature luminescence from a doped QW. Spectrum #25 is taken near QW6 (680°C) and shows a substantially different spectrum. As discussed below, the luminescence from QW6 (measured thickness 3.1 nm with cross-sectional STM) occurs at a wavelength of about 750 nm, but it appears only as a shoulder in this spectrum #25. This indicates that there is substantial diffusion of carriers, and this results in a luminescence signal coming from several QW. This situation is addressed further below. Spectrum #40 is taken over the top three QW. The peak appears at 783 nm and shows the same shape as spectrum #10. Spectrum #55, taken about 5 nm into the cladding layer, shows a peak at 783 nm resulting from electrons recombining in the top QW (QW11), and a peak at 658 nm that originates from the AlGaAs cladding (corresponding to an Al content of x = 37%). This directly demonstrates how injection at a specific position can result in luminescence coming from various locations due to the thermalization and diffusion of the injected carriers.

To further elucidate the effect of thermalization and diffusion on the spectra recorded, it is useful to plot the data in a different way. Figure 5 shows in detail the position-dependent peak wavelengths as squares, and the high and low-energy sides of the peaks at half maximum as circles and triangles, respectively. The expected wavelengths are also shown (diamonds). The QW thicknesses shown in Figure 3 serve as the principal parameter for the wavelength calculation. The differences in wavelength compared to the peak wavelength of the nominally 5-nm-thick QW9, QW10 and QW11 are calculated assuming constant binding energy for the dopants. Starting at position 20 nm, we observe a shift of the peak towards shorter wavelengths. This is expected because the QW become thinner. However, the size of this shift is much smaller than that expected from the calculation shown. This is because the injected carriers thermalize and diffuse, so the spectra represent contributions averaged over several neighboring QW. For an excitation energy of 3.0 eV (1.1 eV above the barrier CB), the thermalization volume is about 30 nm [4], which is comparable to the separation between QW, and diffusion of minority carriers extends this averaging still further. Thus, it is not surprising that the main contribution to the luminescence signal, when we inject carriers into the region around QW6-QW8, does not come from those QW that have a low luminescence yield, but from QW to either side of this region (QW5 and QW9) that have a high luminescence yield. The contributions of QW6-QW8 are only visible as a shoulder on the high-

energy side, as seen in spectrum #25 of Figure 4. Finally, based on the constant peak wavelength of the spectra taken between positions 150 nm and 300 nm, we can confirm that the three nominally identical QW have indeed the same thickness. Furthermore, the energy of the transitions does not change with carriers being injected as hot carriers directly into the QW or into the AlGaAs cladding layer, from where the thermalized electrons have to diffuse back to QW11 first.

For the present data, taken at room temperature, the line shapes are very similar to the ones obtained with conventional photoluminescence. In the region where the excited luminescence originates only from equally thick QW (around QW9, QW10 and QW11) the high-energy side shows exponential decay with $kT \cong 28$ meV, which is typical for room temperature luminescence. On the low-energy side, the decay width is also large, but this is typical for impurity-related transitions in highly doped *p*-type GaAs [5].

Conclusion

We have shown results of STL on GaAs QW and QWR structures including first results of wavelength-resolved STL with nanometer spatial resolution on such structures. The intensity of the luminescence signal depends on the efficiency of carrier injection into the flat-band region and on the competition between radiative and non-radiative processes in this region. The effects of both processes are observed. Importantly, it is the latter process alone that results in lower intensity from the first QW or QWR, indicating that there are defects in these structures due to their proximity to the substrate that reduce the optical efficiency of these structures. The spectra obtained from the QW have the shape expected for room-temperature luminescence from a doped QW. However, for the tunneling conditions used, several of the closely spaced QW contribute to the luminescence signal due to carrier thermalization and diffusion effects, which govern the spatial resolution. These results indicate that STL is a promising technique to measure optical properties of semiconductor nanostructures.

Acknowledgments

This work was supported in part by the Swiss Priority Program in Optics and the Swiss National Science Foundation, contract No. 21/34317.92.

References

[1] Abraham DL, Veider A, Schönenberger CH, Meier H-P, Arent DJ, Alvarado SF (1990) Nanometer resolution in luminescence microscopy of III-V heterostructures. Appl Phys Lett **56**: 1564-1566.

[2] Albrektsen O, Arent DJ, Meier HP, Salemink HWM (1990) Tunneling microscopy and spectroscopy of molecular beam epitaxy grown GaAs-AlGaAs interfaces. Appl Phys Lett **57**: 31-33.

[3] Alvarado SF, Renaud Ph, Abraham DL, Schönenberger CH, Arent DJ, Meier HP (1991) Luminescence in STM on III-V nanostructures. J Vac Sci Technol B **9**: 409-413.

[4] Alvarado SF, Renaud Ph, Meier H-P (1991) High resolution electron beam injection in semiconductors using a scanning tunneling microscope. Journal de Physique IV, Coll. C6 **1** C6-271--C6-275.

[5] Casey HC, Stern F (1976) Concentration-dependent absorption and spontaneous emission of heavily doped GaAs. J Appl Phys **47**: 631-643.

[6] Christen J, Grundmann M, Bimberg D (1991) Scanning cathodoluminescence microscopy: A unique approach to atomic-scale characterization of hetero-interfaces and imaging of semiconductor inhomogeneities. J Vac Sci Technol B **9**: 2358-2368.

[7] Gwo S, Chao K-J, Shih CK, Sadra K, Streetman BG (1993) Direct mapping of electronic structures across $Al_{0.3}Ga_{0.7}As$/GaAs heterojunctions: Band offsets, asymmetrical transition widths, and multiple-valley band structures. Phys Rev Lett **71**: 1883-1886.

[8] Johnson MB, Albrektsen O, Feenstra RM, Salemink HWM (1993) Direct imaging of dopants in GaAs with cross-sectional scanning tunneling microscopy. Appl Phys Lett **63**: 2923-2926.

[9] Marti U, Proctor M, Martin D, Morier-Genoud F, Senior B, Reinhart FK (1991) Fabrication of buried GaAlAs nm-structures by deep UV holographic lithography and MBE growth on finely channelled substrates. Microelectronic Engineering **13**: 391-394.

[10] Montelius L, Pistol M-E, L. Samuelson L (1992) Low-temperature luminescence due to minority carrier injection from the scanning tunneling microscope tip. Ultramicroscopy **42-44**: 210-214.

[11] Pfister M, Johnson MB, Marti U, Alvarado SF, Salemink HWM, Martin D, Morier-Genoud F, Reinhart FK (1994) Atomic structure and luminescence excitation of $GaAs/(AlAs)_n(GaAs)_m$ quantum wires with the scanning tunneling microscope. Appl Phys Lett **65**: 1168-1170.